

# SIMULATED BILAYER from FLOPPY to HOLE and TOPOLOGICAL FLUCTUATIONS.

by  
J. Stecki

Institute of Physical Chemistry, Polish Academy of Sciences,  
ul. Kasprzaka 44/52, 01-224 Warszawa, Poland

November 10, 2018

Abstract.

Simulations of a bilayer in a liquid solvent in the full range of areas from the floppy to the extended state also show the hole/tunnel spontaneous formation. Whether this change of topology is preceded by topological fluctuations of the Gaussian curvature  $K(x, y)$  is an open question. Probability distributions of Gaussian curvature are transformed into those of the ordered inverse radii; these new shapes show a gradual change along the isotherm. The model of Max-Planck group with 5 beads is used, amended to represent amphiphiles in the spirit of the "coarse-grained" or "Martini" force field.

## Introduction.

Simulations of bilayers have greatly extended the knowledge about and the understanding of these prototypes of membranes. Whereas most work was concentrated on the simulation of tensionless bilayers, the wider range of areas was examined as well, beginning with a small interval in the pioneering work of this kind[1], up to the entire range of the existence of a stable bilayer[2-7]. The simplest setup is the liquid system at constant temperature  $T$ , volume  $V$ , and constant  $N$ , the number of amphiphilic molecules, and  $N_s$ , the number of solvent molecules. With change of shape the area  $A$  varies and the lateral tension  $\Gamma$  with it; the "bilayer isotherm"  $\Gamma(A)$  results[2-7]. Its unusual and interesting features are briefly recalled in Section I. One may inquire as to the effect of temperature, but with one exception[7] and another[8] this has not been examined. We show some results elsewhere. With the increase in the area  $A$  at constant temperature, the stretched bilayer eventually gives way but it does so in an interesting manner; it does not break up in droplets or micelles but recedes to keep its surface density and creates a hole – a tunnel – through which the disjointed portions of solvent may connect. Thus the hole is filled with the solvent. The process of such spontaneous formation, without any foreign body attempting to pass through the membrane, has not been studied much by simulation[9]; we examine its appearing on the bilayer isotherm, in relation to the change of Gaussian curvature  $K$ . Normally this quantity is of no interest as it is null and constant, but with the hole formation the genus changes (from the value  $p = -2$  appropriate for system with periodic boundary conditions) and therefore  $K$  changes. Section II is devoted to the Gaussian curvature. An interesting question is whether the sudden creation of hole is preceded by topological fluctuations, fluctuations in  $K$ .

### Section I. The bilayer isotherm and the model used.

Fig.1 shows a bilayer isotherm, the lateral tension  $\Gamma$ , plotted against the specific area per surfactant molecule  $a = 2A/N$ . The main portion of the graph shows the extended bilayer, (EX), where  $\Gamma$  is positive and increasing. Compressed bilayer reaches the tensionless state (which we call the "tensionless state nr.1"); at this area  $a_1$   $\Gamma$  vanishes. On further compression of the area the bilayer undergoes a transition to the "floppy" state (FL). This is the small area of the graph where  $\Gamma$  is negative. Such transitions and the existence of the floppy state are known from experimental studies of vesicles[10] and a counterpart is found here. The surprising feature is the *constancy*

of the *negative*  $\Gamma$ . All this can be understood and qualitatively described by the very simplest theory of undulations as put forward by Helfrich[11]. We have also shown that the scaling with size is predicted by that theory and confirmed the prediction by our simulations of 4 systems of 4 sizes from  $N = 450$  to  $N = 4000$ [4]. Undulations of bilayers have been much studied, for example in[2-12], and the corresponding power spectrum of fluctuations, often under the name of the structure factor,  $S(q)$ , has been determined repeatedly.  $S$  is expected to diverge on vanishing  $q$ ,  $q \rightarrow 0^+$ , as  $1/q^2$  for capillary waves and as  $1/q^4$  for tensionless bilayer (in the "tensionless state nr 2"). Now, upon the transition to the floppy state the asymptote  $q = 0$  is replaced by an asymptote at a positive value of  $q$ ,  $q = q_{as} > 0$  and  $S_{floppy}(q)$  diverges as  $1/(q^2 - q_{as}^2)$ . The region  $q \in (0, q_{as})$  is not accessible. It can be shown[5] that such shift of the  $q$ -asymptote is also predicted by the Helfrich undulation theory. The latter is a heuristic adaptation of the capillary-wave theory but it has been put on a firm footing in a mathematical paper[12] which derives all of it from a microscopic bending hamiltonian, by a coarse-graining procedure. It also follows from that theoretical description that the transition itself is not a true phase transition but a crossover - despite the appearances.

On further compression of the already floppy bilayer there comes a point when the bilayer disintegrates into what appears to be a structureless foam and sometimes a "quad-layer".

The picture described and seen in the left-hand side of Fig.1 is valid for sufficiently large systems. For small bilayers the EX portion of the isotherm continues downwards to large negative values of  $\Gamma$  and then suddenly starts to increase strongly - so that the curve  $\Gamma(a)$  has a spike - and there is no flat section of constant, or nearly constant  $\Gamma$ [4,5]. In our experience at least 1200 amphiphiles were necessary to produce the expected floppy plateau.

The bilayer with the specific area increased above  $a_1$  is in an extended state, gently undulating, with  $\Gamma$  increasing less than linearly, with  $a$ ; then becomes stretched and finally does not disintegrate but recedes and creates a hole. The hole is nearly cylindrical and is filled with the solvent. The first published picture[3] of such a hole already showed that the bilayer recedes keeping its surface area; this was superseded by a more thorough investigation[9]. The lateral tension drops to much lower value. The downward trend of  $d\Gamma/da$  in Fig.1 suggests that perhaps the hole is formed when  $d\Gamma/da = 0$  but on closer scrutiny the plot does not fully support that; the derivative seems to be still positive at

metastable states.

The details of the shape of a bilayer isotherm will depend on the model used and on the details of the intermolecular force field. In Fig.1 we show two sets of points, supplemented by a few points (shown with circles and line) at constant pressure and (slightly) variable density. This is meant to imply that it does not matter very much that we take isochoric data, at constant (overall) density. The main points (Diamonds) were obtained with the additional repulsive force (ARF) mimicking the hydrophobic effect after Goetz et al.[1]; the smaller set of data (Stars) - without that "Deus-ex-machina" addition.

Fig.2 shows a similar isotherm but for molecules with longer 8-bead tails. Since the system is also bigger, the floppy flat portion of  $\Gamma(a)$  is better developed and truly flat.

The model we used in the past was introduced by the Max Planck group[1], as an extension of the very first modelling of amphiphilic molecules - as dimers in a solvent[13]. The liquid system is made of spherical particles, which are either solvent molecules or beads connected in linear chains of unbreakable (chemical) bonds to form amphiphilic molecules. In such a molecule, one terminal bead represents the polar head and the remaining - the nonpolar hydrocarbon chain. Here we use 5 beads (*i.e.* 1 for the head plus 4 for the tail) and exceptionally 9 *i.e.* one for the head and 8 for the linear chain as tail. The intermolecular energy is a sum of pair interactions, all of which are cut and shifted 6-12 Lennard-Jones functions:

$$u(r) = 4\epsilon[(\sigma/r)^{12} - (\sigma/r)^6] \tag{1}$$

In general for 3 species (solvent "s", head "a", and tail-bead "t") the symmetrical matrix of parameters requires 6 energies  $\epsilon_{\alpha\beta}$  and another requires 6 collision diameters  $\sigma_{\alpha\beta}$ . Practically in most if not all simulation work the collision diameters were taken equal for all pairs. Often the energy parameters were also made all equal[1,4,14] as well. Then, as one author noted[14] the molecule was not amphiphilic any more.

Also, an extra term was added to substitute for the absent "hydrophobic force". It is well-known that a hydrocarbon molecule "prefers" its own environment to water and vice versa; it will experience an effective repulsion, in spite of all dispersion forces being attractive. Such an additional repulsive force (ARF) between the solvent "s" and the tail beads "t", has been added[1] and assumed to vary as  $1/r^n$  with  $n = 8$  or  $10$ .

To improve on that model, we note that the essential feature of an amphiphilic molecule is the permanent chemical bonding of two antagonistic groups - a polar (hydrophilic) head and the hydrophobic (non-polar) tail, most often a hydrocarbon tail. Accordingly, we treat these two groups of particles differently. The  $\epsilon$ 's are taken all equal within the non-polar group

$$\epsilon \equiv \epsilon_{tt} = \epsilon_{at} = \epsilon_{st}, \quad (2)$$

and augmented for the "polar group":

$$\epsilon_{ss} = \epsilon_{sa} = \epsilon_{aa} = \omega\epsilon. \quad (3)$$

With  $\omega > 1$  the polar beads "s" and "a" are endowed with a stronger mutual attraction.

In this simple manner the model is improved and the molecule cannot be said "not to be amphiphilic any more". In most of our work we have used the value  $\omega = 2$ . For all intermolecular forces all  $\sigma$ 's are taken equal. The cutoff at distance  $r = 2.5\sigma$  is common to the polar group. Next one manipulates further the potentials after Toxvaerd[15]. All potentials must be shifted if cut, so as to ensure continuity of forces. The  $s$ - $t$  and  $a$ - $t$  forces are made repulsive at all distances by changing the cutoff to  $r = \sigma$  (and therefore the shift to  $+\epsilon$ ). The *intramolecular* bonds are confined to the small neighbourhood of the optimal bond distance by a potential well with infinite barriers[4,15].

Our model can be viewed as a simplified version of the "Martini force field"[16], the latter also named a "coarse grained" model[17].

The Molecular Dynamics simulations were done in the canonical ensemble *i.e.* at constant  $T, V, N$  with Nose-Hoover thermostat.

## Section II. The hole formation and the topological fluctuations.

The spontaneous hole formation in the stretched bilayer is a change of topology. It will affect the Gaussian curvature  $K$ . Whether this sudden change of the surface (and of its genus) is preceded by fluctuations, e.g. by fluctuations of  $K$ , is not known. It is accepted that approaching even a sharp first-order order transition, "the system and its molecules exercise themselves" [18] in preparation to the transition. We have examined the behaviour of  $K$  along the bilayer isotherm reported above. If the Fourier coefficients have been determined, no matter how, one can construct the surface  $h(x, y)$  and from

the definition of  $K$  to obtain  $K(x, y)$ . Total, or overall,  $K_t$  is then

$$K_t = \int_0^L \int_0^L dx dy K(x, y) \quad (4)$$

If a surface is given by the smooth function  $h(x, y)$  in the Monge gauge then

$$K(x, y) \equiv (h_{xx} * h_{yy} - h_{xy}^2)/D^4 \quad (5)$$

where

$$D \equiv \sqrt{1 + h_x^2 + h_y^2} \quad (6)$$

in the usual notation of first and second derivatives of  $h$ . From the Fourier analysis of the simulation data *i.e.* positions of heads,  $h$  is given as a finite sum

$$h(x, y) = a_0/2 + \sum a_n \cos(q_n R_n) + b_n \sin(q_n R_n) \quad (7)$$

where  $q_n$  is a vector  $(2\pi/L)(n_x, n_y)$  and  $R = (x, y)$ . The  $q$ -vectors are usually chosen to fill a square centered at  $(0, 0)$  and a half of it is used in summation, corresponding to the square area  $0 < x < L, 0 < y < L$ . The other curvature, the mean curvature  $H$  is also obtained from  $h(x, y)$  by standard expression, as always with  $D \neq 1$ .

Both were obtained from  $h(x, y)$  at a set of arbitrary values  $(x_j, y_j)$ , chosen as a square grid sufficiently fine for trapezoidal integration. The latter produced the overall total  $K_t$  and total  $H^2$ , their dispersions, and a large set of values of  $K$  at  $(x_j, y_j)$  to be used for the construction of histogram. These computations were done along the entire simulation run and the sets of data obtained were used to construct histograms  $P(K)dK$  and  $P(H^2)d(H^2)$ .

The histograms for  $H^2$  are shown in Figure 3. The mean curvature squared  $H^2$  decays monotonously attaining a rate not too far from an exponential decay in the latest stage of the decay, as can be seen from Figure 3 in semilogarithmic scale. The four points on the isotherm are specified in full detail below; the two upper curves for  $L = 53$  and  $L = 52$  are indistinguishable; that for 46 lies slightly higher than that for 38. The next Figure, Fig.4, shows a portion of the same histograms, near  $H^2 = 0$ . The sequence is the same along the entire histograms (the curves never cross) and the Figure also shows the steep fall very close to  $H^2 = 0$ .

The histograms for  $K$  are more interesting.  $P(K)$  appears as a Dirac delta-function,  $\delta(0)$ , in agreement with the expectation that for a two-dimensional surface with periodic

boundary condition the Euler genus equals -2 and therefore  $K = 0$ . Fig.5 shows the remarkable distributions of  $K$ , in semilogarithmic scale to reveal the broadening of the  $\delta$ -functions.

The nature of the peak is examined in Fig.6 by using a magnified scale; remarkably the discontinuity at  $K = 0$  is approached with a finite slope and with an apparent lack of symmetry about  $K = 0$ . These two features: discontinuity with finite slope and no symmetry, are seen again in Fig.7. It shows the plots of the inverse  $1/P(K)$ , very convenient for the estimation of the slopes and extrapolation to the point of discontinuity. It is not clear if the extrapolation from the left produces the same value as the extrapolation from the right, in view of different slopes and second derivatives. The mathematical representation is an open question; a gaussian distribution is certainly excluded as there is no inflexion in sight. An inverse power is not acceptable either, as the limited plot of Fig.7 already shows.

$K$  was computed often, but not for flat bilayers; rather for those intricate surfaces formed in microemulsions and/or general minimal surfaces(cf.[19,20]). In these nonplanar intricate shapes the Euler index is changed and  $K$  is a most important quantity. There are no known expression for its distribution, even for one of the simplest minimal surfaces[19]. The shapes of those histograms, numerically computed[19], were very similar to those seen in our Figure 5.

With the discontinuity at  $K = 0$  *i.e.* with the part with  $K < 0$  differing from the part with  $K > 0$  the task becomes even more complex. But this will be unnecessary as will become clear.

All histograms as numerical data were obtained for different states of the bilayer, *i.e.* for different areas along the isotherm, Four points were chosen: (1) almost at the tensionless state, (2) in the middle of the isotherm, (3) near the breaking point of stretched bilayer and (4) at the breaking point where the hole-tunnel is formed. The details are as follows:  $T = 1.35, N = 1800, 4$  beads,  $\rho = 0.89$  for 1 points; and then (1)  $L = 38.25, a = 1.62525$ ; (2)  $L = 46.0, a = 2.3511$ ; (3)  $L = 52.0, a = 3.004$ ; and (4)  $L = 53.0, a = 3.1211$ . The last point is the point of hole formation; as mentioned earlier, there is hysteresis. There are metastable states when the hole is not formed for a very long time. for example, starting from the system at  $L = 52.$ , after preliminary equilibration at  $L = 53.$ , running with  $L = 53.$ , we find no hole until  $0.8E6$  timesteps. Then expansion to  $L = 54.$  of the system with newly formed hole, stabilized the tunnel

structure, which on compression back to  $L = 53$ . did not disappear. The earlier part of the data for  $L = 53$ , *i.e.* before the hole was starting to form. were included as (4) and is codenamed as "53h". As is apparent from Fig.1 and 2, the hole formation makes the lateral tension  $\Gamma$  to fall to very different and low values[9].

For examining the approach to state (4) along the bilayer isotherm. *i.e.* in the sequence  $1 \rightarrow 2 \rightarrow 3 \rightarrow 4$  the plot of inverses  $1/P(K)$  appears the best; the peak broadens as seen from Fig.7 but there is no regular pattern.

The lack of symmetry about  $K = 0$  is a disturbing feature. We turn therefore to the origin of these curvatures.

The primary quantities are the *principal radii* of the surface  $h(x, y)$  at that point,  $R_1(x, y)$  and  $R_2(x, y)$ . The principal curvatures are defined as  $c_1 = 1/R_1$  and  $c_2 = 1/R_2$ . The principal radii are obtained as roots of a quadratic equation, usually written in terms of the  $c$ 's

$$a * x^2 + b * x + c == a * (x - c_1)(x - c_2) = 0. \quad (8)$$

As it turns out,  $H$  and  $K$  are related to the roots as

$$H = (1/2)(c_1 + c_2) \quad (9)$$

$$K = c_1 c_2 \quad (10)$$

Therefore  $H$  is simply related to one coefficient in the quadratic equation and  $K$  to the other. Simple algebra produces the solution, the roots, in terms of  $H$  and  $K$ , are

$$c_1 = H - \sqrt{H^2 - K} \quad (11)$$

$$c_2 = H + \sqrt{H^2 - K} \quad (12)$$

In these relations of differential geometry  $H$  and  $K$  are just abbreviations for the combinations of the first and second derivatives of  $h(x, y)$ . Also

$$R_1 = (1/c_1) = c_2/K \quad (13)$$

$$R_2 = (1/c_2) = c_1/K \quad (14)$$

A dump of the  $R$ 's and  $c$ 's followed by the construction of their histograms, revealed interesting features. First, one radius is always very large in absolute value as compared

to the other. This is due to near-planarity of these surfaces. If  $|R_2|$  is  $O(1)$ ,  $|R_1|$  is 10000 or more. However, the signs vary; though  $c_1 < c_2$  always, not necessarily  $|c_1| < |c_2|$  - so the smaller root may be the big one in absolute value and conversely.

The output roots were therefore ordered according to their absolute values: if  $|c_1| < |c_2|$  then  $c_b = c_1$ ,  $c_s = c_2$ , and conversely, if  $|c_1| > |c_2|$  then  $c_b = c_2$ ,  $c_s = c_1$ . The convention is to use the subscript "s" for the *radius* smaller of the two,  $|R_b| > |R_s|$  with  $R_s = 1/c_s$ ,  $R_b = 1/c_b$  and therefore for the larger of the two  $c$ 's. It turns out that which root will produce  $R_b$  and which  $R_s$ , is decided by the sign of  $H$ , the mean curvature. Simply comparing the squares:  $c_2^2 > c_1^2$  if  $H < 0$  and conversely. And the value is

$$(R_s)^{-1} = c_s = (|H| + \sqrt{H^2 - K}) \times H / |H|. \quad (15)$$

The histograms must be now transformed accordingly. First, histograms of unsorted roots  $c_1$  and  $c_2$  are shown in Fig.8, for one point (2) ( $L = 46$ ). A peculiar symmetry appears in that the branch for negative  $K$  is the mirror image of the other histogram for positive  $K$ :

$$P(c_1) = P(-c_2) \quad (16)$$

The test for symmetry is better shown just for the positive semiaxis and with the inverses  $1/P(c_1)$  and  $1/P(c_2)$ , as in Fig.9.

Now the histograms for sorted  $c_s$  and  $c_b$  take a very different look. Fig.10 shows  $P(c_b)$  and  $P(c_s)$ , again for clarity for one state of the bilayer, namely (2) with  $L = 46$ . The larger radius  $R_b$  corresponds to  $c_b$  and  $P(c_b)dc_b$  has a spike at  $K = 0$ ; the smaller radius is  $R_s = 1/c_s$  and  $P(c_s)$  vanishes at  $c_s = 0$  and has a maximum. There is perfect symmetry now between the negative branch and the positive branch *of the same histogram*.  $P(c_s)$  starts linearly from  $P(0) = 0$  with the slope  $(1/4)$ , goes through a maximum and then falls quasi-exponentially; in the final stage  $P \sim const * \exp(-a * x)$ . But as a fitting equation has very limited significance as it is only valid at very large values of the argument. Fig.11 shows the pair from Fig.10 now with semilogarithmic scale. It is seen that  $P(c_s)$  decays almost exponentially, as  $\exp(-\alpha x)$  but with  $\alpha = \alpha(x)$  drifting along the curve to reach its final value at large values of the argument.

The transformations to  $R_s$  and  $R_b$  substantiate and explain in simple terms the curious symmetries seen in Figure 8 but above all remove the lack of symmetries in histograms of  $K$ . The essential point is that it was not enough to use the principal

curvatures  $c_1$  and  $c_2$ ; it is only the curvatures sorted according to their absolute values that had symmetrical histograms. It is physically convincing that the irrelevant big principal radius  $R_b$  and its curvature  $c_b$ , reflecting the overall near-planarity of the surface, were removed. The other and small radius  $R_s$  and its curvature  $c_s$  are the relevant quantities.

Now we compare  $P(c_s)$  for all state points (1)-(4); at last a pattern of regular change appears. As the area per surfactant molecule increases, Fig.12 shows the sharpening of the distribution, a very small insignificant shift of the maximum, and constant initial slope at zero. The decay portion of  $P$  also changes regularly *i.e.* the decay is faster as the distribution gets sharper with the increase in area.

From the histogram one obtains the average  $\langle c_s \rangle$  and its dispersion  $\langle c_s^2 \rangle - \langle c_s \rangle^2$ ; these are shown for all 4 state-points in Fig.13. Just as the histograms  $P(c_s)dc_s$  there is smooth variation except for the additional point at L=38; this is a state point with ARF.

In a related result, the variance of bare  $K$  is shown in Fig.14. Taken as  $\langle KK \rangle - \langle K \rangle \langle K \rangle$ , it shows good regular trends, unlike all untransformed histograms. Because  $K = c_1 c_2$ ,  $K^2$  will be  $c_1^2 c_2^2 = c_s^2 c_b^2$  and apparently the regular variation of  $c_s^2$  is not spoiled much by the presence of  $1/R_{big}^2$ . Note that  $\langle K \rangle$  may be slightly off its true value of nil; we take  $D \neq 1$  so that  $K(x, y)$  does not vanish identically as it does in the small gradient approximation  $D = 1$ .

As mentioned earlier, it would be an unnecessary and tedious exercise to try to find a mathematicla representation fot the listograms of  $K$ . Also, even for one of the simplest minimal surfaces, this is not known[19]. Now, for the symmetric  $P(c_s)dc_s$ , it appears that a function

$$P(x) \sim x \exp[-\alpha x^n] \quad (x \geq 0) \quad (17)$$

(with a mirror image for  $x \leq 0$ ) is not too far away, esp. for portions away from the maximum of  $P$ . However, this attempt was not fully successful, as different least-square values for  $n$  were obtained:  $n = 0.668$ ,  $n = 1$  , and  $n = 1.12, 1.25$ . Trying to impose  $n = 1$  for all was clearly not correct. And the maximum was not perfectly reproduced. Therefore a satisfactory mathematical representation, even for  $P(c_s)$ , was not found.

These results have some further consequences of minor nature. The linear combination  $c_1 + c_2$  or  $c_1 - c_2$  will be often swamped by the root bigger in absolute value and

therefore might not be very useful. We note that the quantity  $H^2 - K = (1/4)(c_1 - c_2)^2$  is always positive, so that the quadratic equation always has real roots and never complex roots.

As the histograms of  $c_s$  were shown above, those for the radii,  $P(R_s)dR_s$ , are not shown because their plots do not bring anything new.

### Summary and Discussion.

We have found a new transformation of the curvatures  $H$  and  $K$ , the mean and the Gaussian, to quantities with exactly symmetric (about zero) histograms and varying smoothly along the bilayer isotherm.

The numerical results were shown for 4 selected state points along the bilayer isotherm, one near the tensionless state no.1, one in the middle of the isotherm, one almost at the breaking point of hole formation, and one (metastable state) exactly at the hole formation. The data - positions of heads on both monolayers - were collected from simulation runs at  $T, V, N$ , one run producing e.g. 7600 data sets.

The untransformed histograms - probability distributions -  $P(H^2)d(H^2)$  and  $P(K)dK$ , were examined and their plots are shown in the Figures. Their features led to reexamination of the derivation of these curvatures, as it is given in standard differential geometry; a new transformation resulted. In it, the principal radii are sorted according to their magnitude irrespectively of sign. This ordering is crucial; it is not sufficient to introduce principal curvatures  $c_1$  and  $c_2$ .

These new objects,  $c_s = 1/R_s$  and  $c_b = 1/R_b$ , have symmetrical probability distributions which also vary smoothly along the isotherm.

The resulting pattern of variation along the isotherm, can be interpreted by recalling that along the isotherm  $\Gamma(a)$ , with the increase of the specific area  $a$  the bilayer is gradually stretched. Therefore predictably stretching impairs strong fluctuations of the monolayers and of the bilayer as a whole. Thus the distributions shown in Fig.12 have smaller probability of large argument for the bilayer more strongly stretched. Similarly the dispersions fall with  $a$ , as shown by Fig.13 and Fig.14.

There is no premonition of the breaking of the bilayer surface by creation of a hole - it appears to be a catastrophe without warning. As pointed out in the introduction, it is quite a special phenomenon, when the bilayer spontaneously recedes, trying to keep its structure and surface density, and makes room for a tunnel, the latter immediately

filled with solvent molecules.

### Acknowledgements.

The author is greatly indebted to Dr John Nagle (Pittsburgh) for a discussion, but particularly to Dr O.Edholm (Stockholm) for several extensive discussions which led the author to undertake this particular investigation. He thanks the Institute of Physical Chemistry of the Pol. Acad. Sci. for their continuing support.

### References

- [1] R. Goetz and R. Lipowsky, J. Chem. Phys. 108, 7397 (1998).
- [2] J. Stecki, Int. J. Thermophys. 22, 175(2001).
- [3] J. Stecki, J. Chem. Phys. 120, 3508 (2004).
- [4] J. Stecki, J. Chem. Phys. 122,111102(2005).
- [5] J. Stecki, J. Chem. Phys. 125, 154902 (2006);arXiv.0412248  
available as of Dec.10,2004. see also J.Phys.Chem. B112(14),4246(2008).
- [6] W. K. den Otter, J. Chem. Phys. 123, 214906 (2005).
- [7] H. Noguchi and G. Gompper, Phys. Rev.E73, 021903 (2006).
- [8] E. Lindahl and O.Edholm, J. Chem. Phys.113,3882(2000)
- [9] see however I. R. Cooke and M.Deserno, J. Chem. Phys.123,224710(2005).
- [10] E. Evans and W. Rawicz, Phys. Rev. Lett. 64,2094(1990).
- [11] W. Helfrich and R. M. Servuss, Nuovo Cimento 3D, 137 (1984); see also W. Helfrich,  
in *Les Houches, Session XLVIII, 1988, Liquids at Interfaces* (Elsevier, New York,  
1989).
- [12] A.Adjari, J.-B. Fournier, and L.Peliti, Phys. Rev. Lett.86,4970(2001).
- [13] B. Smit Phys. Rev. A 37, 3431 (1988)
- [14] A. Imparato, J. C. Shilcock, and R. Lipowsky, Eur. Phys. J. E11, 21 (2003)
- [15] e.g. Paz Padilla and Soeren Toxvaerd, J. Chem. Phys.106,2342(1997).
- [16] S.J.Marrinck, A.H.de Vries, and A.E.Mark, J.Phys.Chem.B108,750(2003).
- [17] E. G.Brandt, A.R.Brown, J.N.Sachs, J.F.Nagle, and O.Edholm, Biophysical Journal 100, 2104 (2011) and Supplement.

- [18] B. Widom, at the Amsterdam IUPAP Conf. on Statistical Mechanics, 1973.
- [19] U. S. Schwarz and G. Gompper, Phys. Rev. Lett.85,1472(2000) where references to related work can be found.
- [20] R. Holyst and W.Gozdz, in Encyclopedia of Applied Physics, Wiley-VCH, Weinheim 1999, pp 146-160, where references to earlier work can be found.

### Figure Captions.

A short Caption is put under each Figure.

In all Figures the scales are arbitrary with one exception of normalized distribution in Fig.12.

FIG.1. Bilayer isotherm  $T=1.35$ , 4+1 beads, w/ extra force(Diamonds) and without (Stars); Circles -  $P = \text{const}$ .

FIG.2. Isotherm  $T=1.35$  with (Diamonds) and without(Stars) the extra-force AFR; Boxes mark runs with holes. 8+1 beads.

FIG.3.  $P(H^2)d(H^2)$  for  $L=53(\text{hole}), 52, 46, 38$ .

FIG.4.  $P(H^2)d(H^2)$  for  $L=53(\text{hole}), 52, 46, 38$ .

FIG.5. Histograms of Gaussian K for  $L=38, 46, 52, 53, 53h$ .

FIG.6. Selected peaks of Gaussian K;  $L=46(+), 52(\text{Stars}), 53h(\text{Circles})$  and estd. maximum -line.

FIG.7. Inverse of  $P(K)$  near peaks:  $L=38(+), 46(\text{Stars}), 53(\text{Circles}), 53h(\text{Filled Circles})$ . No pattern, no symmetry.

FIG.8. Principal curvatures;  $L=46$ .

FIG.9. Symmetries for principal curvatures. Proof that  $P(c_1) = P(-c_2)$ .

FIG.10. Sorted roots (principal curvatures); the radius  $R_b$  is bigger in absolute value;  $c_b = 1/R_b$  - Plus signs,  $c_s = 1/R_s$  - Stars.

FIG.11. Sorted roots (principal curvatures); the radius  $R_b$  is bigger in absolute value;  $c_b = 1/R_b$  - Plus signs,  $c_s = 1/R_s$  - Stars.

FIG.12.  $P(c_s)$  normalized to  $(1/2)$ , with  $R_s$  being the smaller in absolute value;  
 $L = 38$ (Boxes),  $L = 46$ (Plus signs),  $L = 53$ (Stars).

FIG.13. Curvature  $c = 1/R_{sm}$ ;  $\langle c \rangle$ (Diamonds),  $\langle c^2 \rangle$ (Stars),  $\langle (c - \langle c \rangle)^2 \rangle$  (Boxes).

FIG.14. Dispersions for H(Stars), H(sm.grad.)(Circles), K(Boxes).

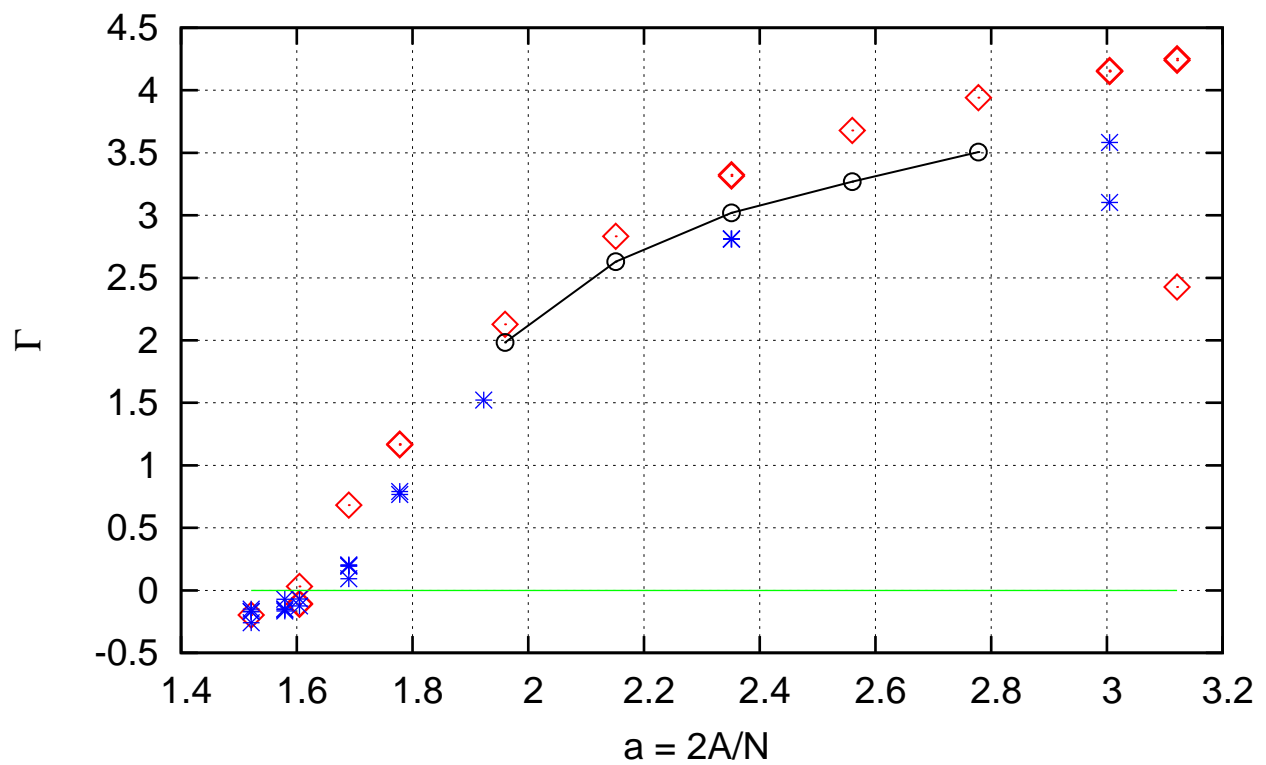


FIG.1. Bilayer isotherm  $T=1.35$ ,  $4+1$  beads, w/ extra force (Diamonds) and without (Stars); Circles -  $P=\text{const}$ .

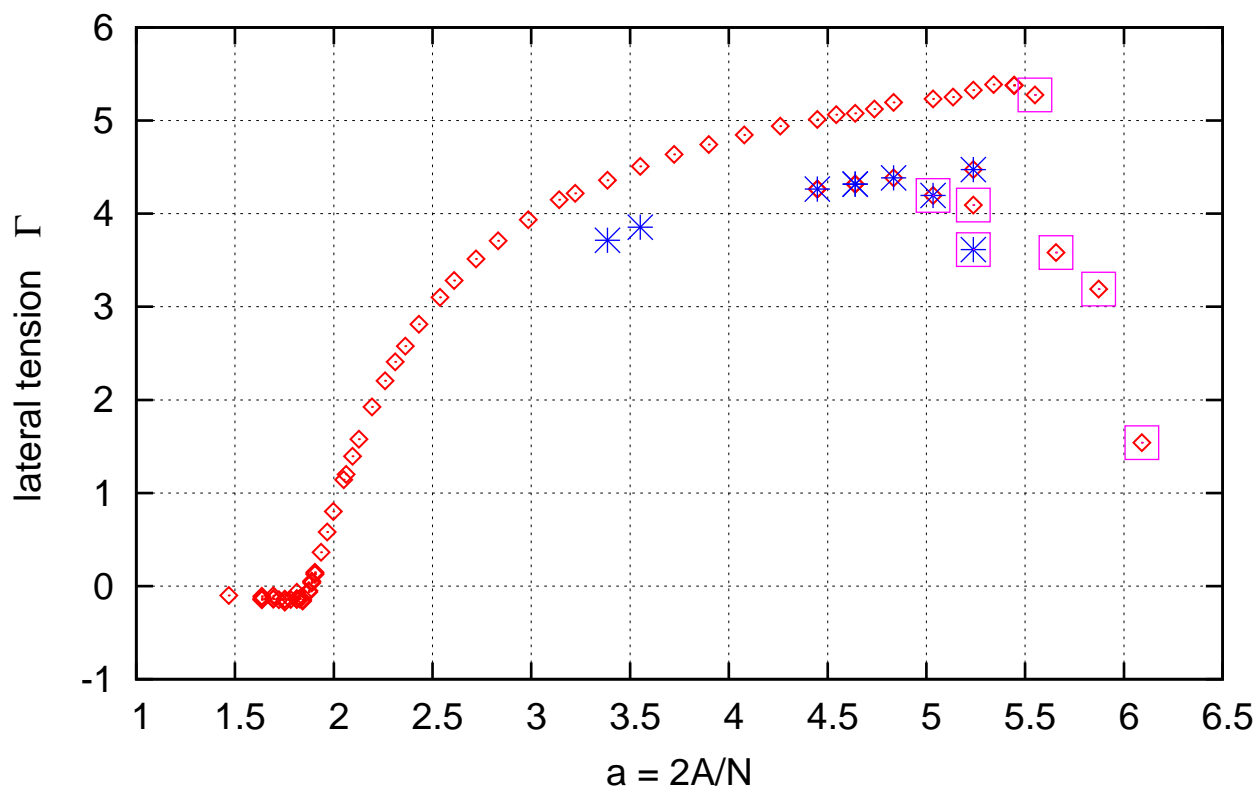


FIG.2. Isotherm  $T=1.35$  with (Diamonds) and without (Stars) extra-force; Boxes mark runs with holes.  $8+1$  beads.

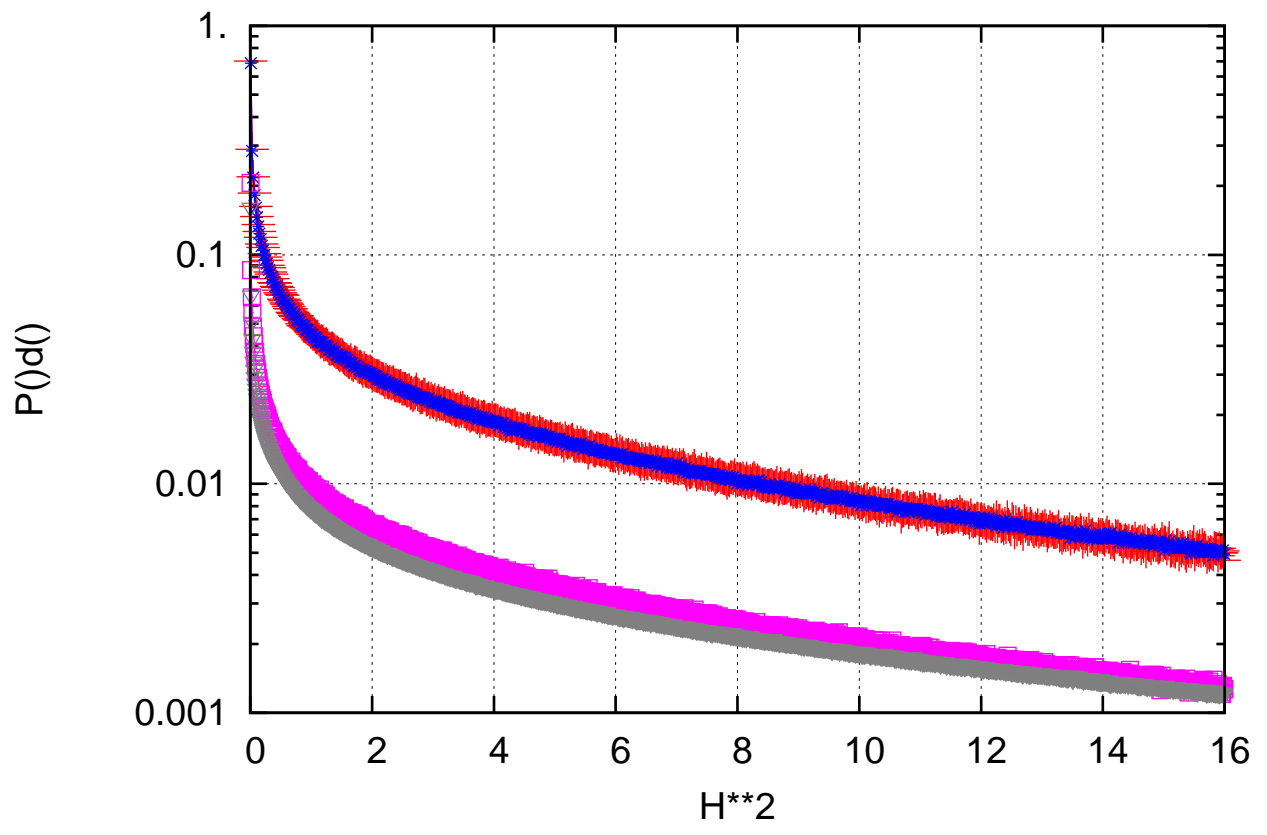


FIG.3.  $P(H^2)d(H^2)$  for  $L=53(\text{hole}), 52, 46, 38$

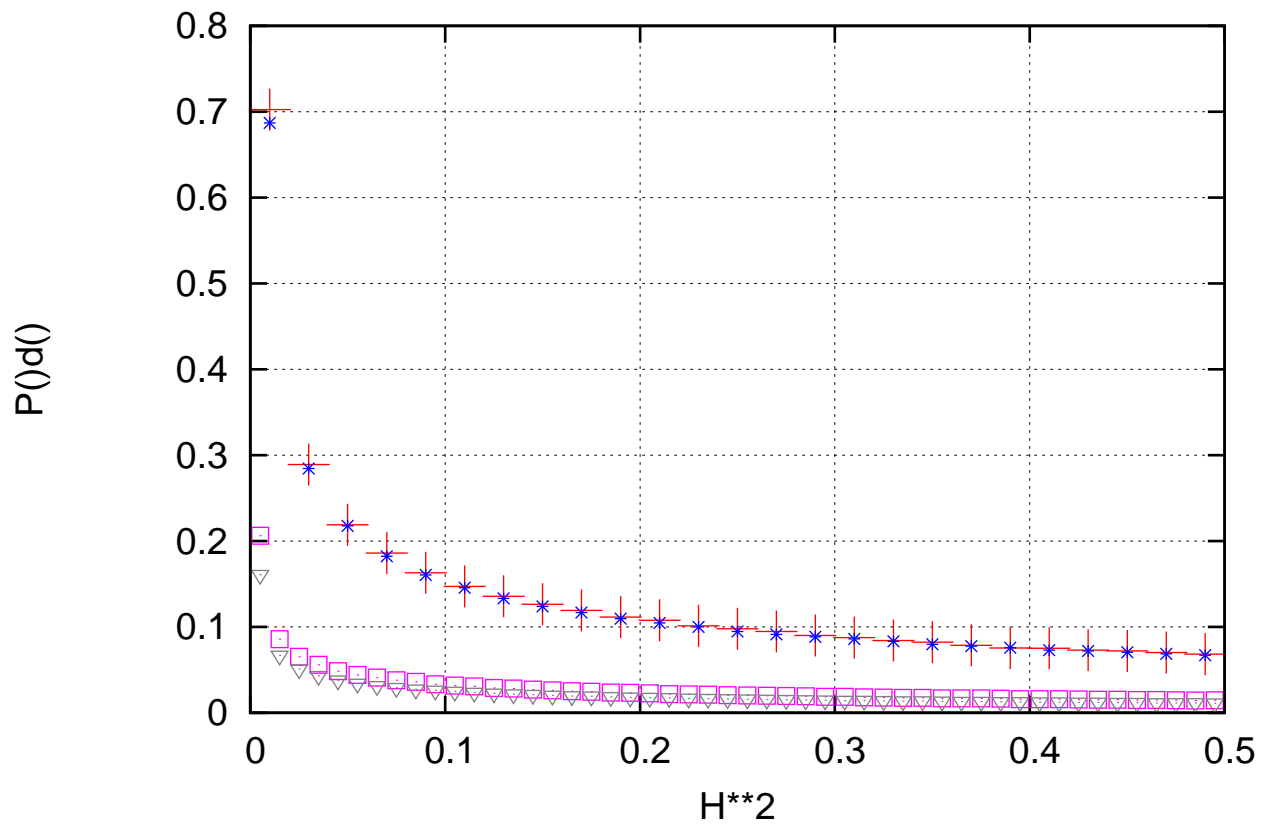


FIG.4.  $P(H^2)d(H^2)$  for  $L=53(\text{hole}), 52, 46, 38$

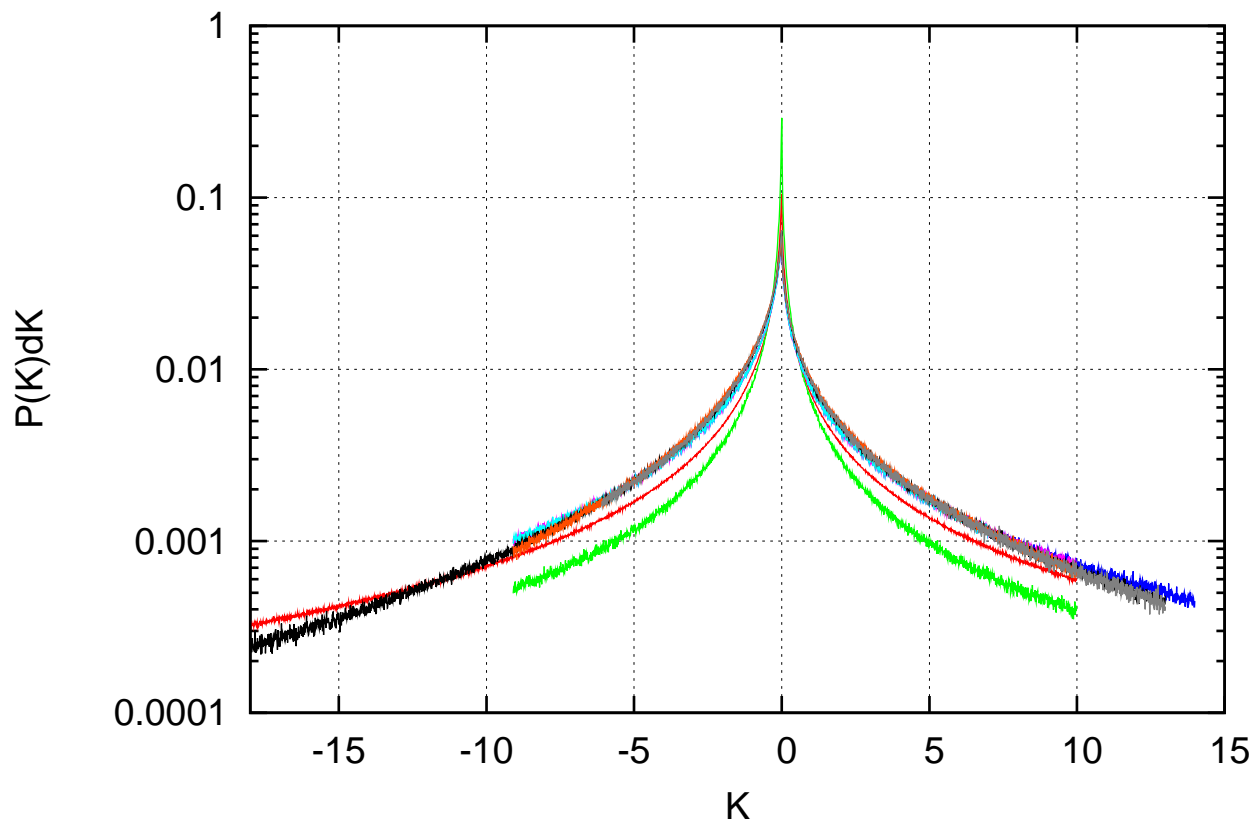


FIG.5. Histograms of Gaussian  $K$  for  $L=38,46,52,53,53h$

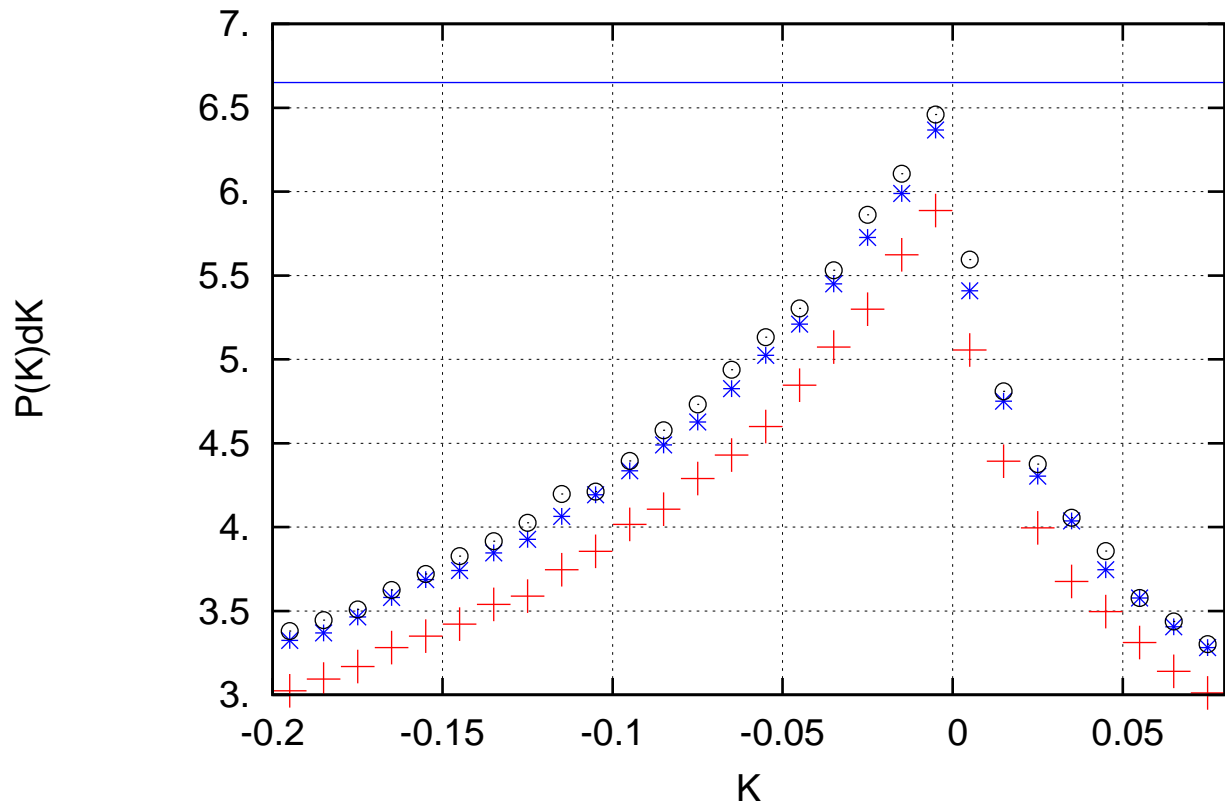


FIG.6. Selected peaks of Gaussian K;  
 L=46(+),52(Stars),53h(Circles and estd. maximum -line)

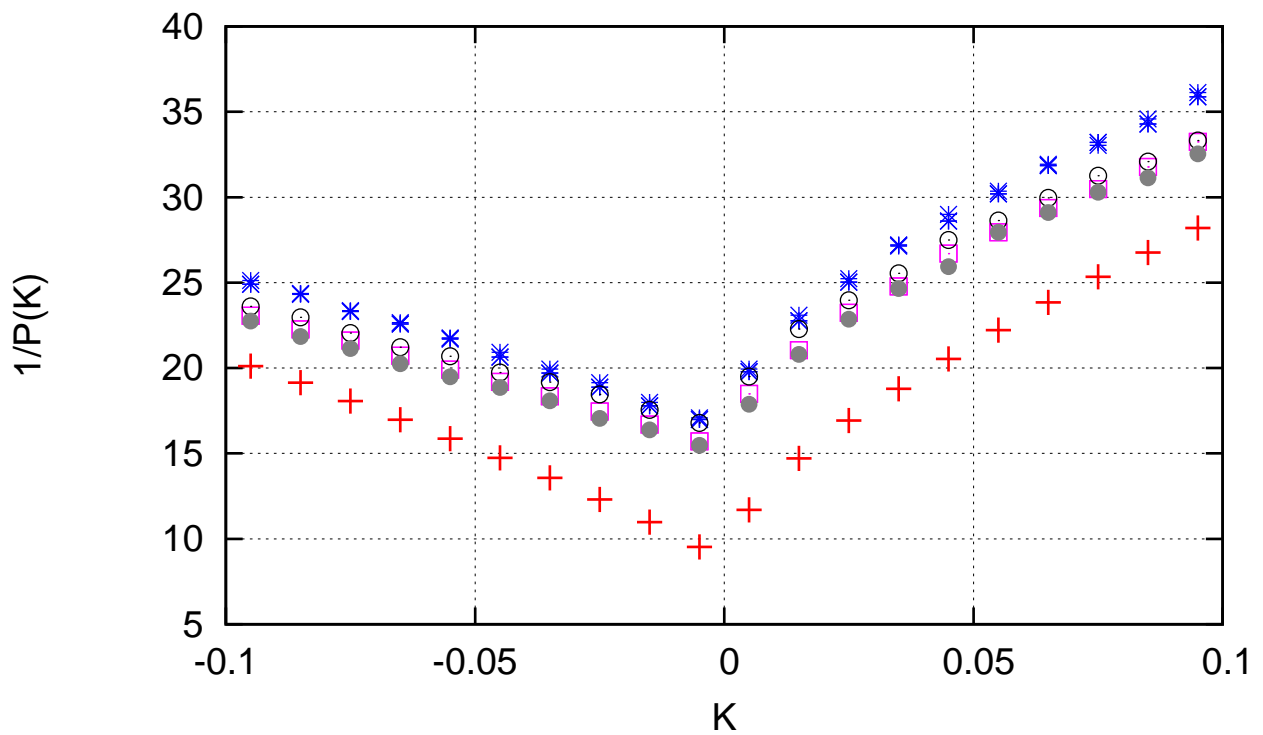


FIG.7. Inverse of  $P(K)$  near peaks:  $L=38(+)$ ,  $46(\text{Stars})$ ,  $53(\text{Circles})$ ,  $53h(\text{Filled Circles})$ . No pattern, no symmetry.

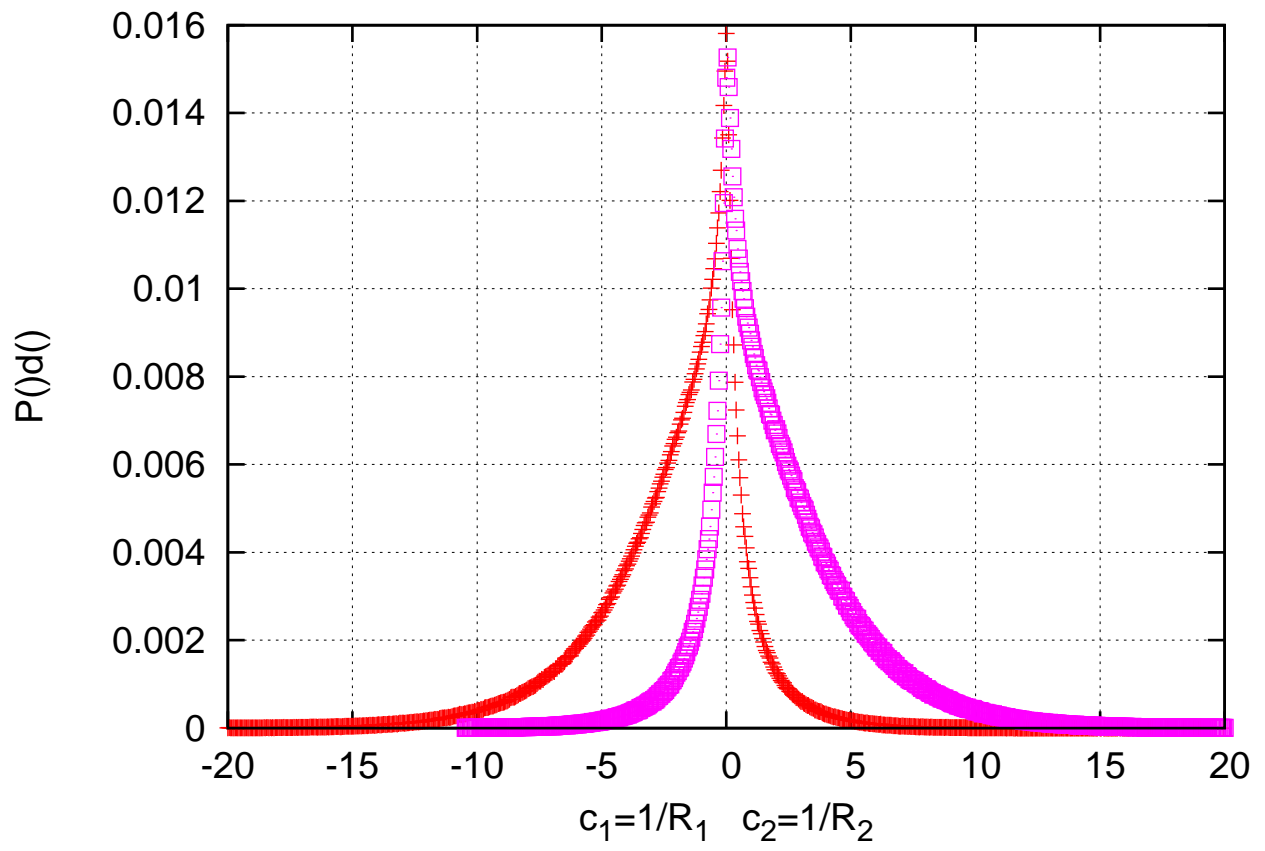


FIG.8.Principal curvatures; L=46

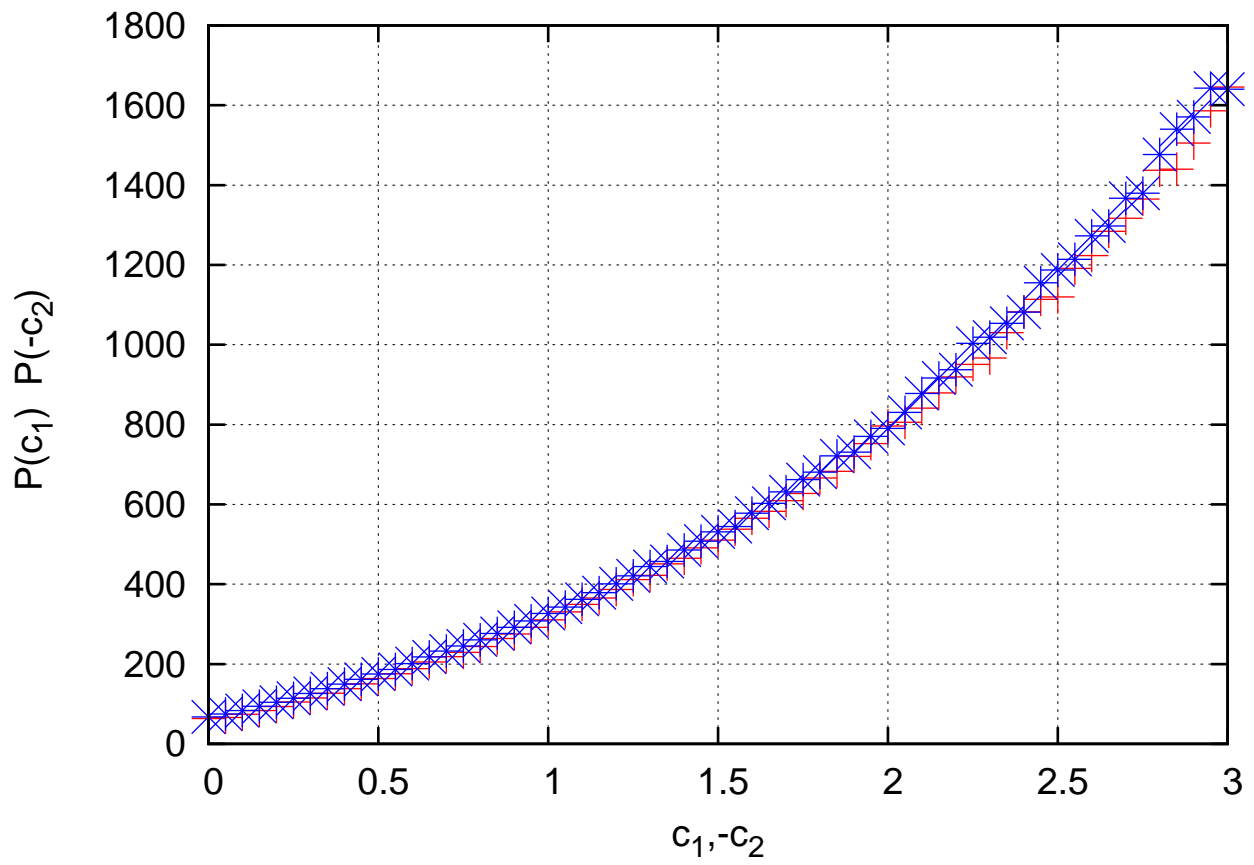


FIG.9.Symmetries for principal curvatures.

Proof that  $P(c_1) = P(-c_2)$  and conversely

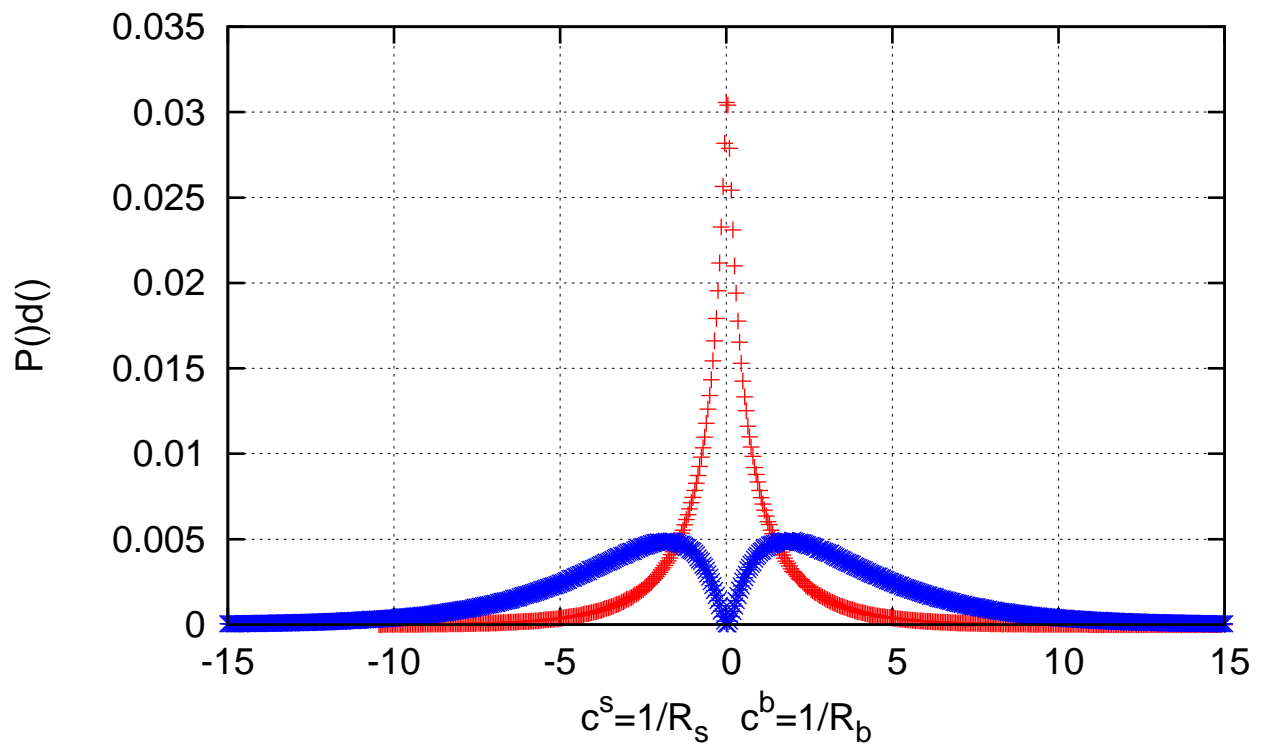


FIG.10.Sorted roots (principal curvatures); the radius  $R_b$  is bigger in absolute value;

$c^b=1/R_b$  - Plus signs,  $c^s=1/R_s$  - Stars

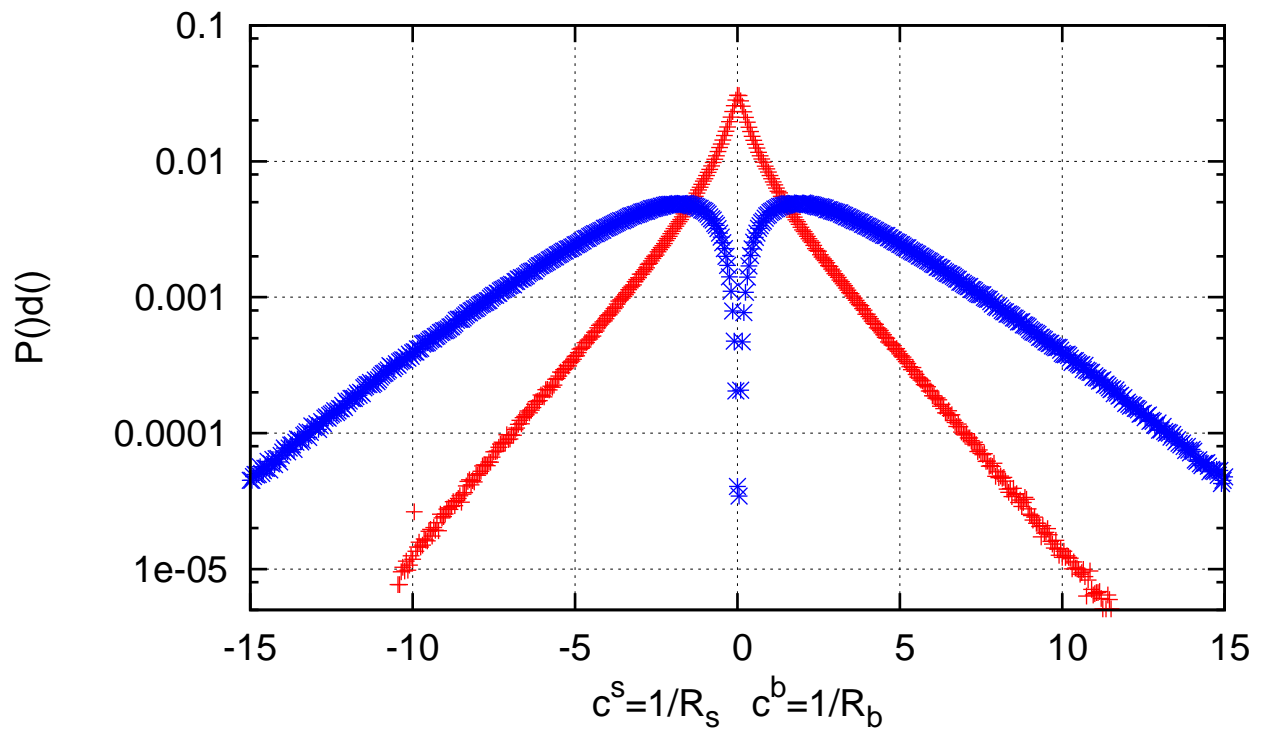


FIG.11. Sorted roots (principal curvatures); the radius  $R_b$  is bigger in absolute value;  
 $c_s=1/R_s$  - Plus signs,  $c_b=1/R_b$  - Stars

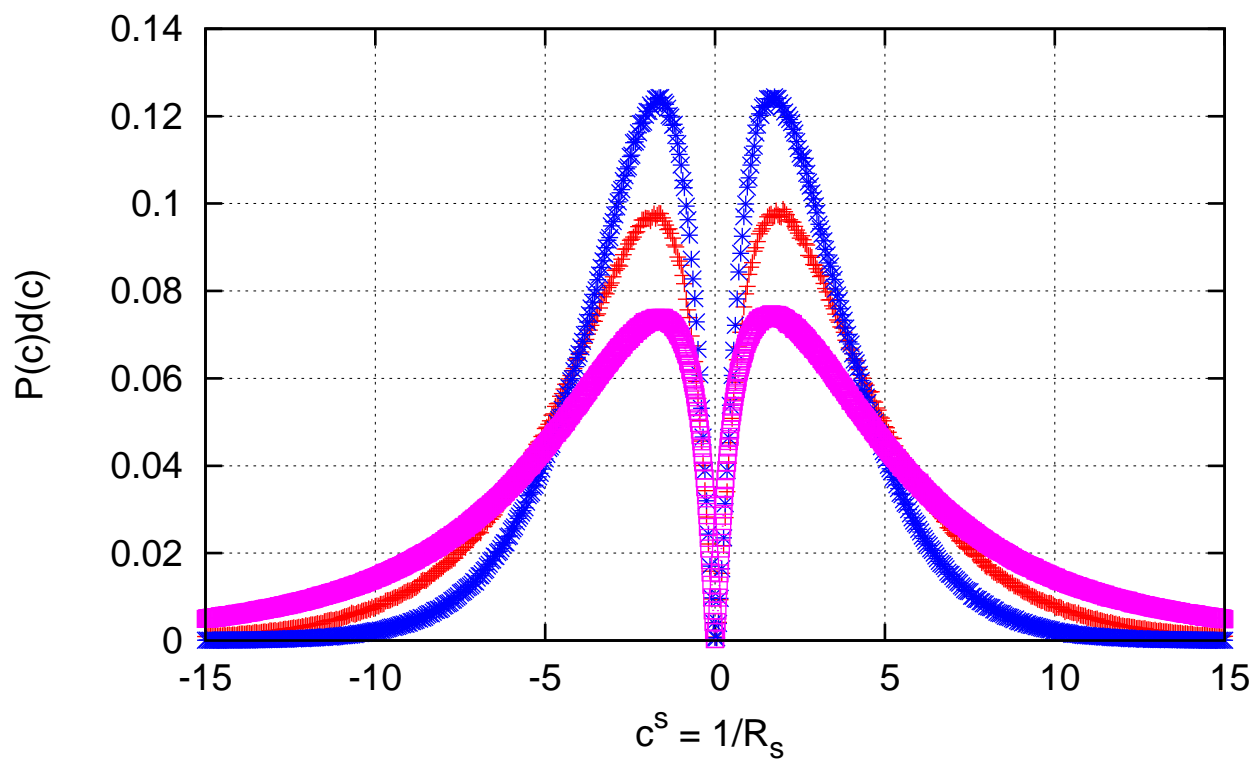


FIG.12.  $P(c^s)$  normalized to  $(1/2)$  with  $R_s$  being the smaller in the absolute value;  $L=38$ (Boxes),  $46$ (Plus signs),  $53$ (stars)

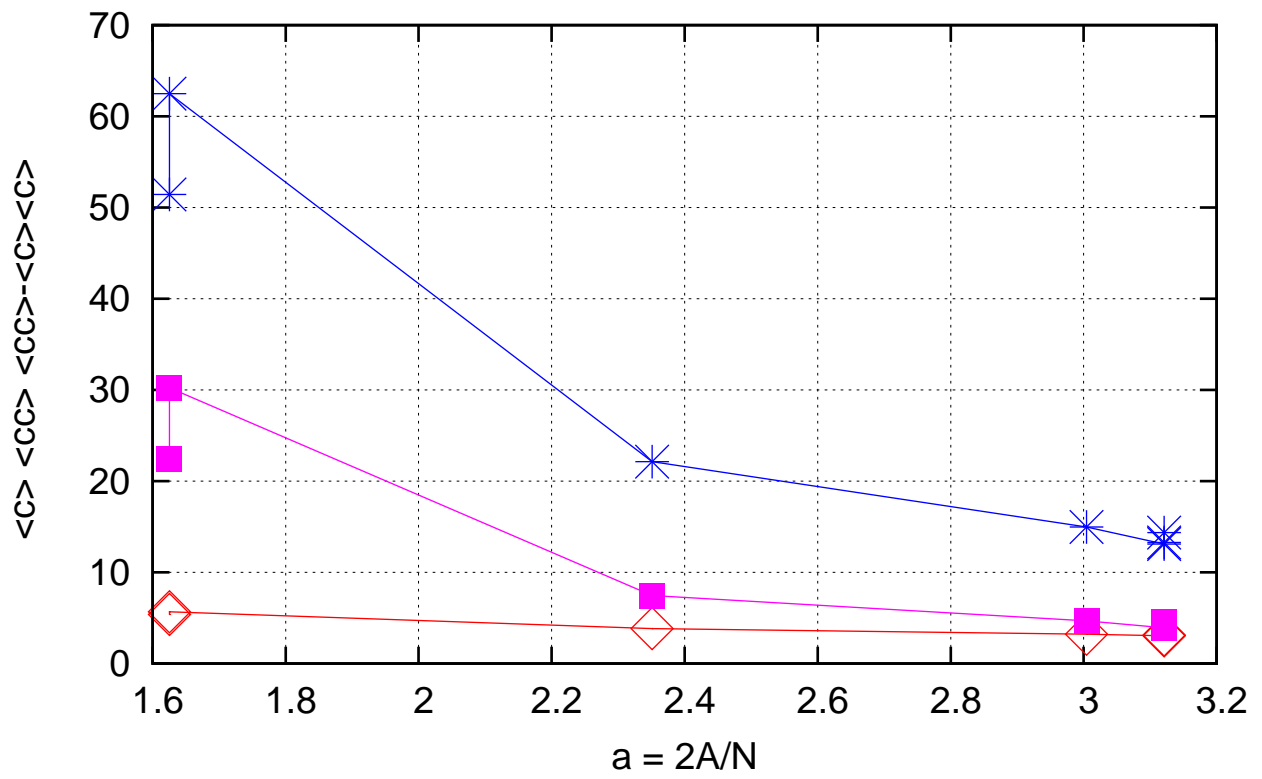


FIG.13. Curvature  $c=1/R_{sm}$ ; average  $\langle c \rangle$  (Diamonds),  $\langle c^2 \rangle$  (Stars), and dispersion  $\langle (c - \langle c \rangle)^2 \rangle$  (Boxes)

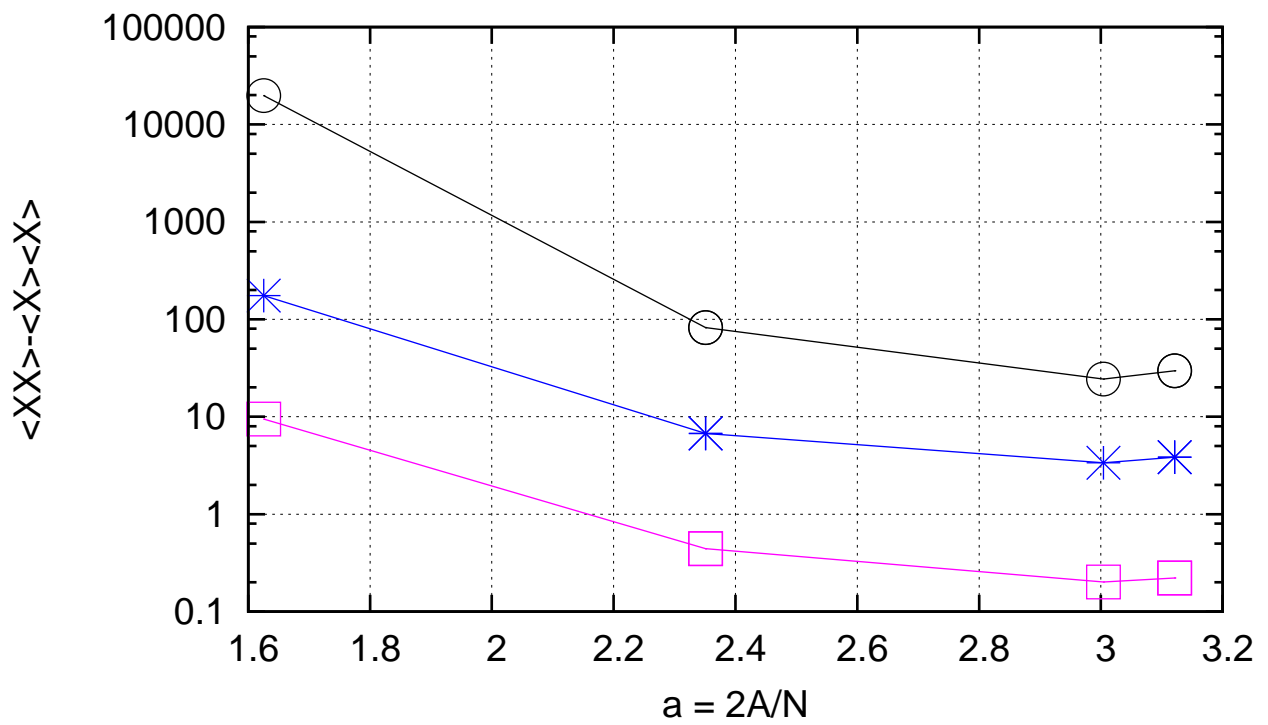


FIG.14. Dispersions for H(Stars), Hsm.grad.(Circles), K(boxes)